Thermal structure of low-grade accreted Lower Cretaceous distal turbidites, the Central Pontides, Turkey: insights for tectonic thickening of an accretionary wedge

Mesut AYGÜL[1,2,*], Aral I. OKAY[1], Roland OBERHÄNSLI[2], Martin A. ZIEMANN[2]
[1]Eurasia Institute of Earth Sciences, İstanbul Technical University, Maslak, İstanbul, Turkey
[2]Institute of Earth and Environmental Science, University of Potsdam, Potsdam-Golm, Germany

Abstract: Albian-Turonian subduction-accretionary complexes are exposed widely in the Central Pontides. A major portion of the accretionary complexes is made up of a metaflysch sequence consisting of slate/phyllite and metasandstone intercalation with blocks of marble, Na-amphibole bearing metabasite, and serpentinite. The metaflysch sequence represents distal parts of a large Lower Cretaceous submarine turbidite fan deposited on the Laurasian active continental margin that was subsequently accreted and metamorphosed during the Albian. Raman spectra of carbonaceous material of the metapelitic rocks revealed that the metaflysch consists of metamorphic packets with distinct peak metamorphic temperatures. The majority of the metapelites are low-temperature (ca. 330°C) slates characterized by lack of differentiation of the graphite (G) and D2 defect bands. They possibly represent offscraped distal turbidites along the toe of the Albian accretionary wedge. Other phyllites are characterized by a slightly pronounced G band with a D2 defect band occurring on its shoulder. Peak metamorphic temperatures of these phyllites are constrained to 370–385 °C. The phyllites are associated with a strip of incipient blueschist facies metabasites and are found as a sliver within the offscraped distal turbidites. We interpret the phyllites as underplated continental sediments together with oceanic crustal basalt along the basal décollement. Tectonic emplacement of the underplated rocks into the offscraped distal turbidites was possibly achieved by out-of-sequence thrusting causing tectonic thickening and uplift of the wedge.

Key words: Pontides, distal turbidites, offscraping, underplating, low-grade metamorphism, graphitization, Raman microspectroscopy

1. Introduction

Accretionary wedges form along the sinking oceanic lithosphere by tectonic accumulation of detrital sediments and oceanic crustal rocks with pelagic sediments causing ocean-ward tectonic growth of the continental domains (von Huene and Scholl, 1991; Moore et al., 2001). Tectonic frontal accretion is achieved by mainly scraping off trench-fill turbidites as imbricated packages and underplating them along the basal décollement beneath the offscraped part of the wedge (Karig and Sharman, 1975; Platt, 1986; Sample and Fischer, 1986; Kimura and Ludden, 1995). The wedges can reach several hundred kilometers in width at active continental margins when there is a high amount of sediment supply into trench, as in the Makran (e.g., Platt et al., 1985; McCall, 2002).

In the Central Pontides, northern Turkey, Albian-Turonian subduction-accretionary complexes are exposed over large areas forming part of the former Laurasian active continental margin (Okay et al., 2013; Aygül et al.,

2015a). To the north, the wedge is characterized by the presence of voluminous accreted terrigenous metaclastic rocks underlain by a high-pressure/low-temperature (HP/LT) metabasite- and micaschist-dominated metamorphic sequence along a synsubduction extensional shear zone. The accreted metaclastic rocks consist of slate/phyllite and metasandstone intercalation with extensive blocks of marble, incipient blueschist facies metabasite and serpentinite representing the accreted distal part of a large Lower Cretaceous turbidite fan deposited on the Laurasian active continental margin and subsequently accreted (Okay et al., 2013; Aygül et al., 2015a). Hence, the Central Pontides provide a natural laboratory for a better understanding of the accretionary processes under a high amount of sediment flux into the trench.

The majority of the clastic sedimentary rocks contain primary organic matter consisting of a mixture of C, H, O, N, and S known as kerogen (e.g., Tissot and Welte, 1978). With increasing metamorphic temperature, the weakly

* Correspondence: aygulm@itu.edu.tr

ordered atomic structure of the kerogens transforms into the well-ordered graphite called graphitization (Landis, 1971; Diessel et al., 1978; Itaya, 1981; Beyssac et al., 2002b). Raman spectrometry is possibly the most efficient method for revealing the degree of graphitization of the carbonaceous material (Pasteris and Wopenka, 1991; Wopenka and Pasteris, 1993; Yui et al., 1996). Recently, calibrations of Raman spectra of carbonaceous material (RSCM) allow derivation of precise temperature constraints on metapelitic rocks (Beyssac et al., 2002a; Rahl et al., 2005; Aoya et al., 2010; Lahfid et al., 2010). It is particularly efficient in low-grade metamorphism where index minerals are generally absent for conventional geothermobarometric methods (Beyssac et al., 2004, 2007).

We performed RSCM measurements on the metapelitic rocks of the low-grade HP accreted distal turbidites in order to unveil the thermal structure of the relatively shallow parts of the Albian-Turonian wedge. The obtained thermal fabrics of the accreted distal turbidites also provide new insights on tectonic growth of the wedge.

2. Geological setting
The Pontides represent part of the Mesozoic active continental margin of Laurasia (Meijers et al., 2010;

Okay and Nikishin, 2015). It was rifted from the Eurasian mainland by the opening of the Black Sea as a back-arc basin during the Late Cretaceous (Figure 1; Okay et al., 1994; Okay and Tüysüz, 1999). In the central part of the Pontides two distinct tectonic units have been identified, the İstanbul and Sakarya zones. The İstanbul Zone consists of a crystalline basement of Neo-Proterozoic age (Chen et al., 2002) overlain unconformably by Early Ordovician-Devonian sedimentary rocks (Figure 2; Boztuğ, 1992; Dean et al., 2000). The Sakarya Zone is represented by a Permo-Carboniferous Variscan basement (Nzegge et al., 2006; Okay et al., 2015) and Upper Triassic siliciclastic turbidites with Triassic limestone olistoliths (Ustaömer and Robertson, 1993, 1994, 1997; Okay et al., 2015). Middle Jurassic arc-related granitoids extensively cut the basement rocks of the Sakarya Zone (Yılmaz and Boztuğ, 1986; Okay et al., 2014). The granitoids are associated with LP/HT metamorphic rocks forming part of deep levels of a Middle Jurassic arc. An associated Middle Jurassic subduction-accretionary complex is reported in NE Turkey (Topuz et al., 2013). Upper Jurassic limestones and Lower Cretaceous turbidites unconformably overlie the underlying sequences (Tüysüz, 1999; Okay et al., 2013).

The Lower Cretaceous turbidites, known as the Çağlayan Formation, form an arc shaped submarine fan
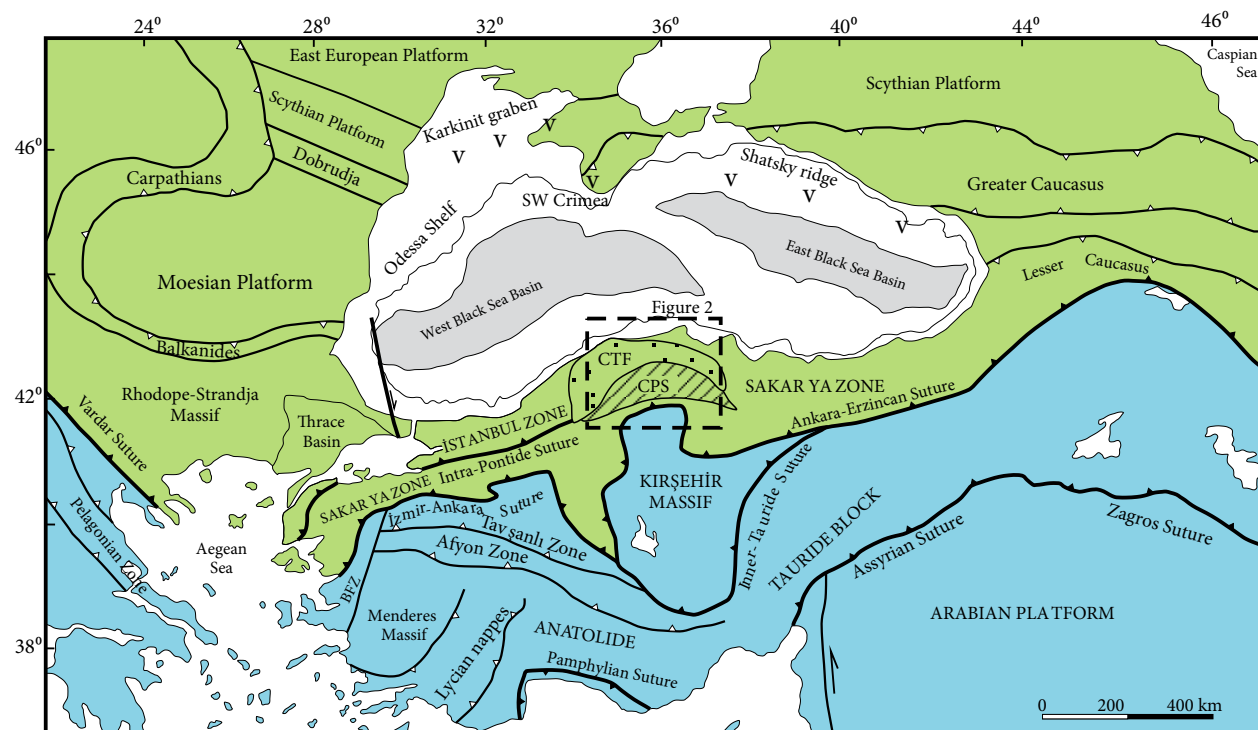
Figure 1. Tectonic map of Turkey and surrounding regions modified from Okay and Tüysüz (1999). Laurasian units are shown in green and Gondwana-derived terranes in pale blue. CPS: Central Pontide Supercomplex, CTF: Lower Cretaceous submarine turbidite fan. North of the Black Sea, "V" marks the Albian volcanic arc modified from Nikishin et al. (2015).
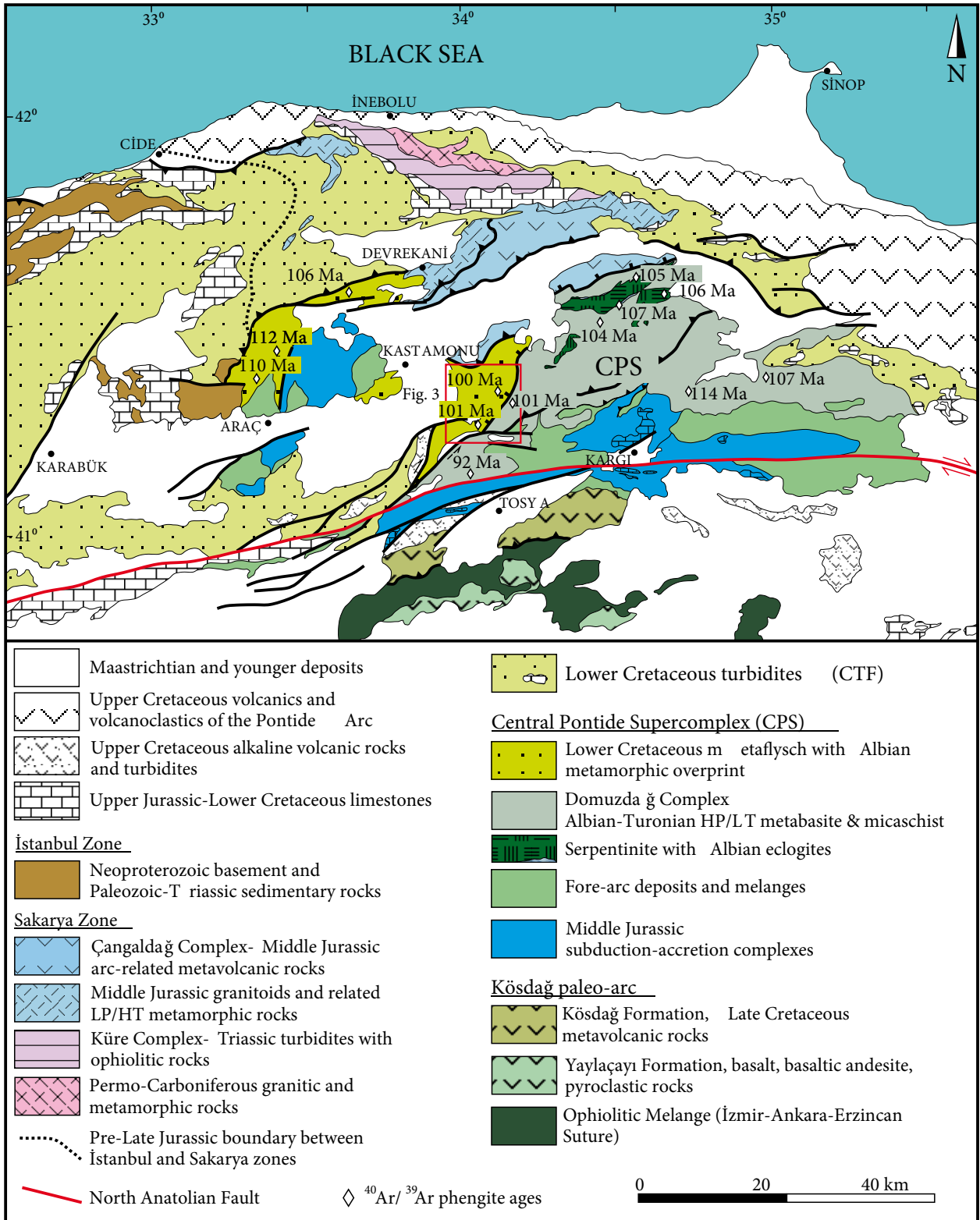
Figure 2. Geological map of the Central Pontides modified from Tüysüz (1990), Uğuz et al. (2002), Okay et al. (2013, 2014), and Aygül et al. (2015a, 2015b).

consisting of sandstone and dark shale intercalation with a large number of blocks. The blocks comprise Upper Jurassic-Lower Cretaceous shallow marine limestones and lesser amounts of Paleozoic sandstones derived from the underlying sequences of the İstanbul Zone (Figure 2). Based on its nannofossil contents, the Çağlayan Formation is assigned a Barremian-Aptian age (Hippolyte et al., 2010). A Lower Cretaceous depositional age is further supported by detrital zircons (Okay et al., 2013). The Çağlayan Formation is interpreted as synrift deposits related to the opening of the Black Sea basin (Görür, 1988; Hippolyte et al., 2010). Detrital zircons from the turbidites, however, indicate a major source area in the East European Craton and Scythian Platform north of the Black Sea implying that the Black Sea basin opened after Early Cretaceous time (Okay et al., 2013).

To the south of the Lower Cretaceous turbidites, Middle Jurassic and Cretaceous subduction-accretionary complexes, the Central Pontide Supercomplex (CPS), crop out over a large area (Figure 2; Okay et al., 2013; Marroni et al., 2014; Aygül et al., 2015a). The Cretaceous accretionary wedge consists of HP/LT metamorphic rocks of continental and oceanic origin, fore-arc deposits, and mélanges. The oceanic unit, known as the Domuzdağ Complex, consists mainly of eclogite to blueschist facies metabasite and micaschist with serpentinites, metagabbro, metachert, and marble representing deep levels of the subduction-accretionary complexes (Tüysüz, 1990; Ustaömer and Robertson, 1993, 1994, 1999; Altherr et al., 2004; Okay et al., 2006, 2013; Aygül et al., 2015a). ^{40}Ar/^{39}Ar phengite ages from the Domuzdağ Complex range between 114 and 92 Ma (Okay et al., 2006, 2013; Aygül et al., 2015a). An associated Albian arc is reported north of the Black Sea (Figure 1; Nikishin et al., 2015). The CPS is locally unconformably overlain by an Upper Cretaceous volcanosedimentary sequence representing fore-arc deposits (Okay et al., 2006, 2013; Tüysüz and Tekin, 2007). The volcanosedimentary sequence passes upward a mélange-like unit consisting mainly of ophiolitic blocks. To the south, the CPS is structurally underlain by an accreted Late Cretaceous intraoceanic arc (Figure 2; Aygül et al., 2015b).

2.1. Accreted Lower Cretaceous distal turbidites

The accretionary continental unit of the Albian-Turonian wedge is a metaflysch sequence consisting mainly of slate/phyllite and metasandstone intercalations with marble, metabasite, and serpentinite blocks. There are two main exposures of the metaflysch units: i) the Martin Complex exposed NW of Araç with a contact with Lower Cretaceous turbidites, and ii) the Esenler Unit exposed further southeast of Kastamonu (Figures 2 and 3). While the Martin Complex is characterized by greenschist facies metamorphism, the Esenler Unit contains metabasites

showing incipient blueschist facies metamorphism. ^{40}Ar/^{39}Ar phengite dating on the metaflysch units constrains the regional HP metamorphism to 112–100 Ma (Albian) (Okay et al., 2013; Aygül et al., 2015a). Clastic zircon studies on the Martin Complex reveal that it represents metamorphosed equivalents of the Lower Cretaceous turbidite fan (Okay et al., 2013). It is inferred that the Esenler Unit represents the accreted distal part of the fan deposited on the Laurasian active continental margin.

In the studied area, the Esenler Unit consists predominantly of an alternation of weakly recrystallized slate and metasandstone (Figure 4a). Foliation is defined by fine-grain white mica in the slates and detrital quartz is partly retained (Figures 5a and 5b). Close to the contacts, slates transform into phyllites (Figure 4b). They have larger grain size and show spaced foliation defined by white mica and quartz (Figures 5c and 5d). The nature of this slate to phyllite transition is not clear. Debris flow levels consisting of pebble to boulder-size recrystallized limestone blocks occur within the metaflysch sequence (Figure 4c). These gravity-driven recrystallized limestone blocks can reach up to 200 m across. Lower Cretaceous fossils were reported from the recrystallized limestones (Barkurt et al., 1990). Serpentinites are exposed along shear zones together with phyllite (Figure 4d). In the accreted distal turbidites, the only metamorphic constraint is obtained from a metabasite lens exposed northwest of the studied area within a serpentinite-rich tectonic zone (211B in Figure 3). The metabasite consists of crossitic Na-amphibole, calcic-amphibole, sodic-pyroxene, epidote, chlorite, albite, and titanite. The metamorphic conditions were weakly constrained to 7–12 kbar pressure and 400 ± 70 °C temperature by conventional geothermobarometric methods (Aygül et al., 2015a).

Hemipelagic siltstone-shale intercalation together with pillow lava and radiolarite blocks cropped out as a tectonic sliver within the Esenler Unit (Figure 3). The contact between this Kirazbaşı Complex and the Esenler Unit is possibly controlled by back-thrusting prior to the generation of the extensional shear zone. To the north, the metaflysch sequence is overthrust by low-grade metavolcanic units and, to the southeast, it is underlain by the oceanic HP/LT metamorphic sequence along a synsubduction extensional shear zone (Aygül et al., 2015a). To the south, however, post-Eocene oblique strike-slip faults overprint the extensional shear zone and underthrust the Esenler Unit beneath the Domuzdağ Complex.

In this study, we performed RSCM on 15 metapelitic rocks of the Esenler Unit in order to uncover the thermal structure of the accreted distal turbidites. The samples were collected along sections vertical to the general structural
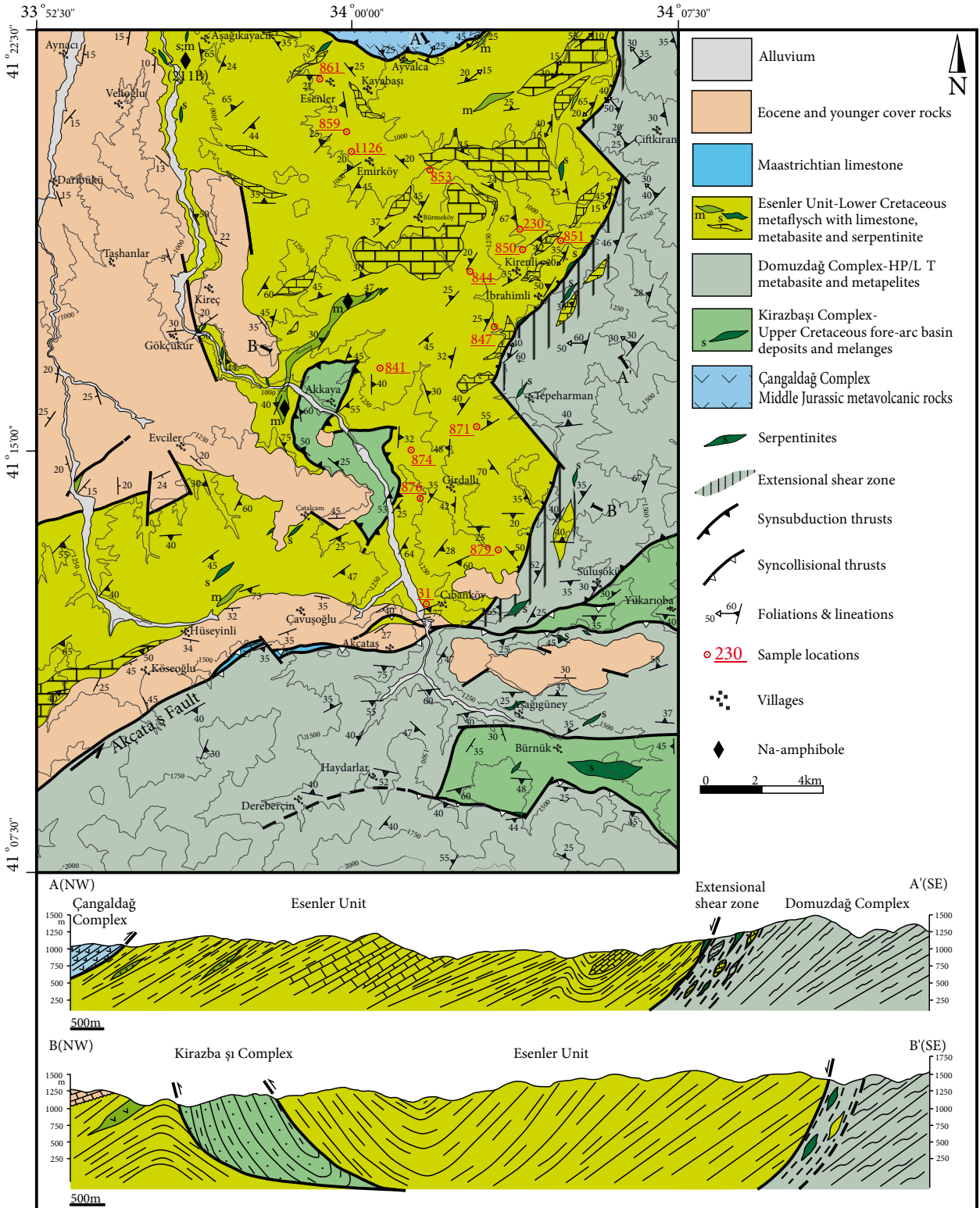
Figure 3. Geological map of the area studied with geological cross-sections (modified from Aygül et al., 2015a).
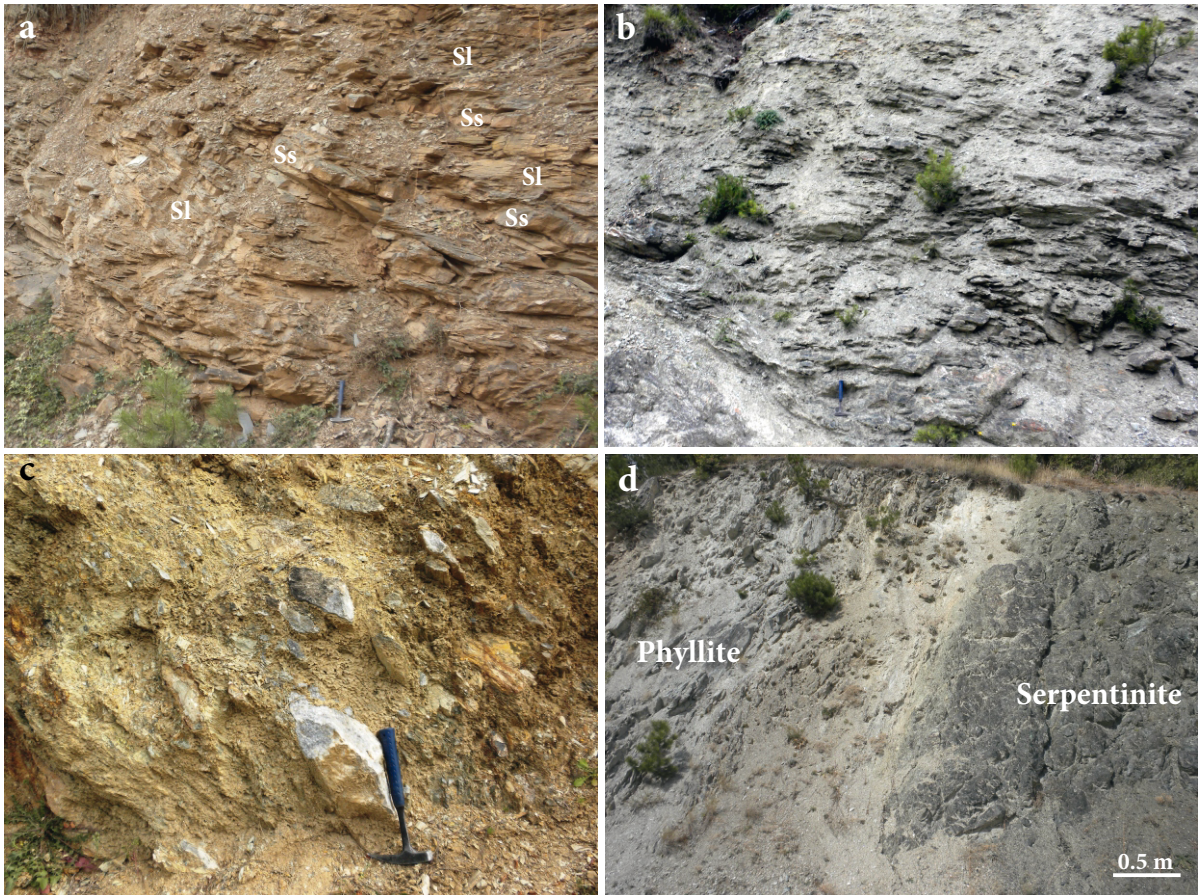
Figure 4. Field photos of the accreted distal turbidites. **a)** Slate (*Sl*) and metasandstone (*Ss*) intercalation. **b)** Phyllites. **c)** A debris flow level consisting of various sized marble olistoliths. **d)** A serpentinite slice within the phyllites on the main Kastamonu-Tosya road.

trends of the Albian-Turonian wedge and comprise both slate and phyllites (Figure 3; Table 1). The obtained temperature data might also allow us to understand the structure of the wedge itself.

3. Methodology

Raman microspectroscopy on carbonaceous material was performed at the Raman Laboratory of the Institute of Earth and Environmental Sciences at Potsdam University using a confocal, edge filter-based spectrometer (LabRam HR 800, HORIBA Jobin Yvon) with a Nd:YAG laser for excitation at a wavelength of 532 nm. Measurements were performed in situ on polished thin sections. Thin sections of the samples were cut orthogonal to the foliation and parallel to stretching lineation. Carbonaceous particles were measured below transparent minerals like quartz, albite, and white mica to exclude influences of polishing-related mechanical destruction of the carbonaceous material structure (Figure 6; Pasteris, 1989; Beyssac et al., 2002b; Scharf et al., 2013). Twenty to 30 points were measured for

each of the samples with an acquisition time of 120 s. Some of the analyzed points, however, were eliminated due to contamination with epoxy. The measured Raman spectra of the carbonaceous material were decomposed for all Raman peaks of carbon by using PeakFit (v4.12) software. A Voight function was used for fitting of the Raman bands. Fitting procedures were applied to the 1000–2000 cm^{-1} interval of the Raman range, which contains the first-order region of the Raman spectrum (Tuinstra and Koenig, 1970; Nemanich and Solin, 1979). The first-order region (1100–1800 cm^{-1}) hosts the main G band (fully ordered graphite band, at 1580 cm^{-1}) with disordered or defect (D) bands including D1 at 1350 cm^{-1} and D2 at 1620 cm^{-1}. Broad defect bands of D3 (at 1500 cm^{-1}) and D4 (at 1200 cm^{-1}) occur in carbonaceous material at low temperatures with very poorly ordered atomic structure (Beyssac et al., 2002a, 2002b; Sadezky et al., 2005; Lahfid et al., 2010). For temperature calculations two empirical calibrations were used. The calibration of Beyssac et al. (2002a) uses the R2 ratio of integral intensities of the bands [(D1 / (G + D1 +
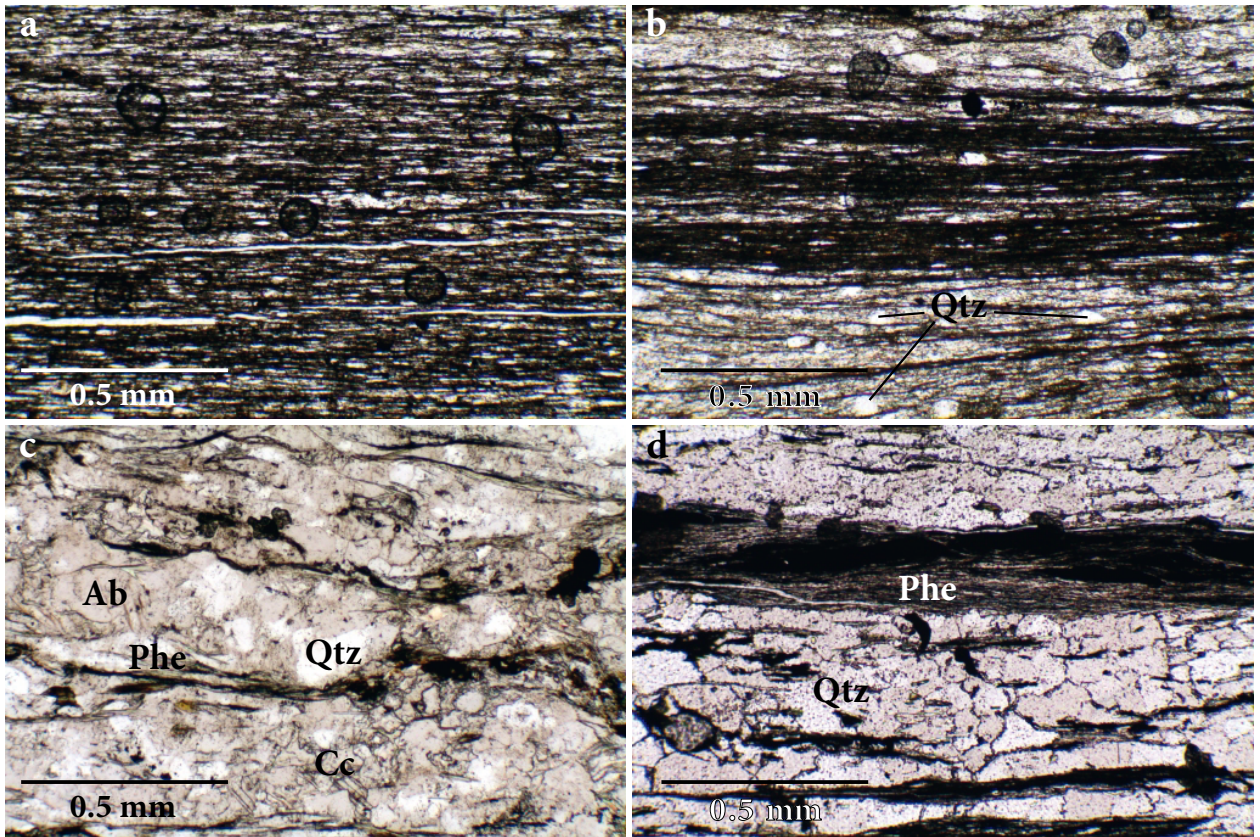
Figure 5. Representative photomicrographs of the metapelitic rocks (plane polarized light). **a & b)** Fine-grained slates (samples 847 and 853). Foliation is defined by white mica and partly recrystallized detrital quartz. **c & d)** Coarser-grained phyllites with spaced foliation (samples 31 and 879). Ab = albite, Qtz = quartz, Phe = phengite, Cc = calcite.

Table 1. UTM coordinates (European 1979 Datum) of the analyzed metapelitic samples.

Sample	x	y
31	36T 05 86007	45 61629
230	36T 05 88842	45 74615
850	36T 05 89035	45 73738
844	36T 05 87373	45 72916
879	36T 05 88350	45 63831
871	36T 05 87976	45 68095
876	36T 05 85922	45 65761
874	36T 05 85489	45 67304
841	36T 05 84538	45 69821
847	36T 05 88172	45 71385
851	36T 05 90262	45 74020
853	36T 05 86097	45 76405
1126	36T 05 83817	45 77178
859	36T 05 83350	45 77637
861	36T 05 82426	45 79377

D2))$_A$] and is applicable for the temperature range of 330–650 °C. Rahl et al. (2005) presented a modified calibration using both R1 [(D1/G)$_H$] and R2 ratios extending the temperature range between 100 and 700 °C. Both calibrations are reported to have ±50 °C error range. In this study, we provide the temperature values obtained from both calibrations. However, we mainly built our study on the temperature values obtained from the method of Rahl et al. (2005) due to the fact that it is essentially calibrated for low-grade metamorphic rocks. Since graphitization is an irreversible process, the RSCM method gives the peak metamorphic temperatures (Pasteris and Wopenka, 1991; Beyssac et al., 2002a).

4. RSCM of the low-grade accreted distal turbidites

The metapelitic rocks of the Esenler Unit exhibit variable Raman spectra indicating distinct degrees of graphitization and peak metamorphic conditions (Figure 7). Two groups can be identified generally. The first group forms the majority of the measured samples in which the G and D2 defect bands are found as a single band near 1600 cm^{-1}. After decomposing, the positions of the bands are 1595
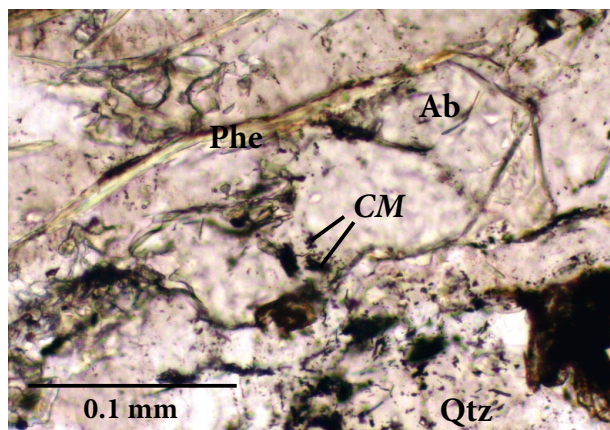
Figure 6. A photomicrograph in plane polarized light showing carbonaceous material (CM) within albite and quartz. Ab = albite, Qtz = quartz, Phe = phengite.

cm^{-1} (G) and 1614 cm^{-1} (D2), respectively (Figure 8a). The D1 defect band occurs at 1345 cm^{-1}. This group is also characterized by D3 and D4 defect bands with high intensities. These bands generally cause an upward shift of the spectrum including G, D1, and D2 bands. The D3 band was located mostly between 1520 cm^{-1} and 1530 cm^{-1} and the D4 band between 1230 cm^{-1} and 1245 cm^{-1} (Figure 8a). One sample (871) differs from the rest by its low intensities of D3 and D4 defect bands (Figure 7).

The second group is characterized by the differentiation of the graphite (G) and D2 defect peaks and the absence of D3 and D4 defect bands (Figure 7). The G band occurs at 1588–1590 cm^{-1} and the D2 defect band is placed as a shoulder of the G band around 1618–1620 cm^{-1} (Figure 8b). The D1 band of these samples is located at ca. 1352 cm^{-1}.

The analytical data and calculated mean temperatures of the samples are given in the Table 2. In accordance with the Raman spectra, the lowest temperature values are obtained from the samples with indistinguishable G and D2 bands (the first group). For these samples, while the calibration of Rahl et al. (2005) reveals ca. 330 °C temperature, the calibration of Beyssac et al. (2002a) estimates slightly higher temperatures of ca. 345 °C.

The second group with slightly pronounced G bands gives higher peak metamorphic temperatures. The calibrations of Beyssac et al. (2002a) and Rahl et al. (2005) indicate temperatures of 370–355 °C and 381–367 °C, respectively. A comparison diagram of the temperatures obtained by the two calibrations is shown in Figure 9.

5. Discussion

Accreted distal turbidites form a major portion of the Albian-Turonian accretionary wedge of the Central
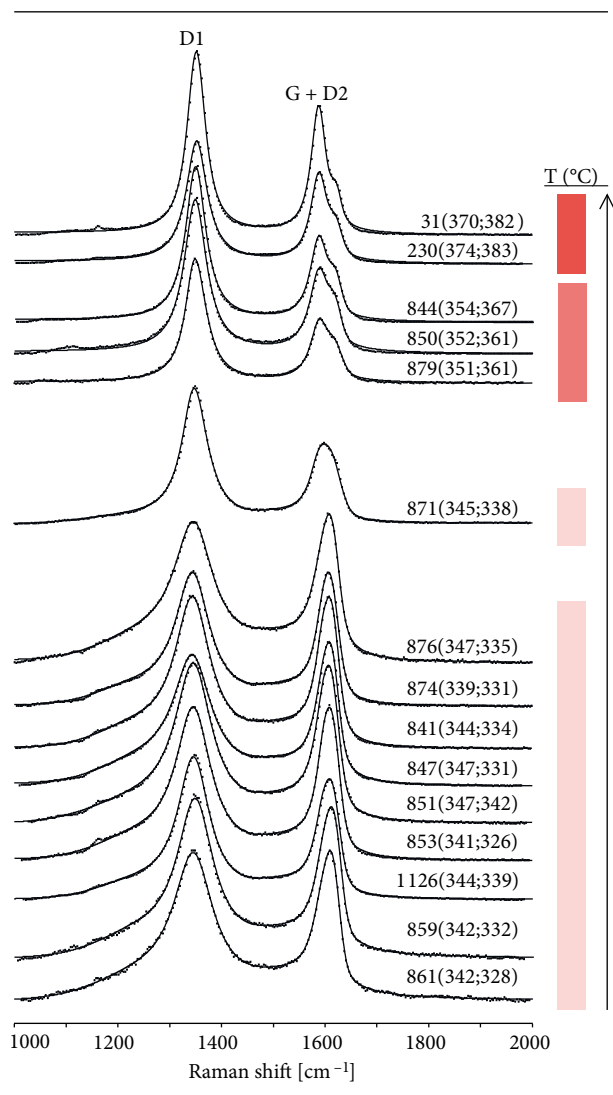
Figure 7. Representative Raman spectra of carbonaceous material from the accreted distal turbidites. Two groups can be identified. The majority of the samples are characterized by absence of a clear G band. Sample 871 represents gradual increasing of temperature within this group. The second group exhibits a slightly pronounced G band. Temperature values of individual spectra are given in parentheses based on the calibrations of Beyssac et al. (2002a) and Rahl et al. (2005), respectively.

Pontides. They represent accretionary tectonic growth of the Laurasian active continental margin under high clastic supply into a trench in which a large Lower Cretaceous submarine turbidite fan formed (Okay et al., 2013; Aygül et al., 2015a). The uniform lithology of the accreted turbidite sequence, however, makes recognition of structural elements like major faults difficult. Besides, due to the rheological weakness of the slate and phyllites, the primary structural framework can be easily overprinted
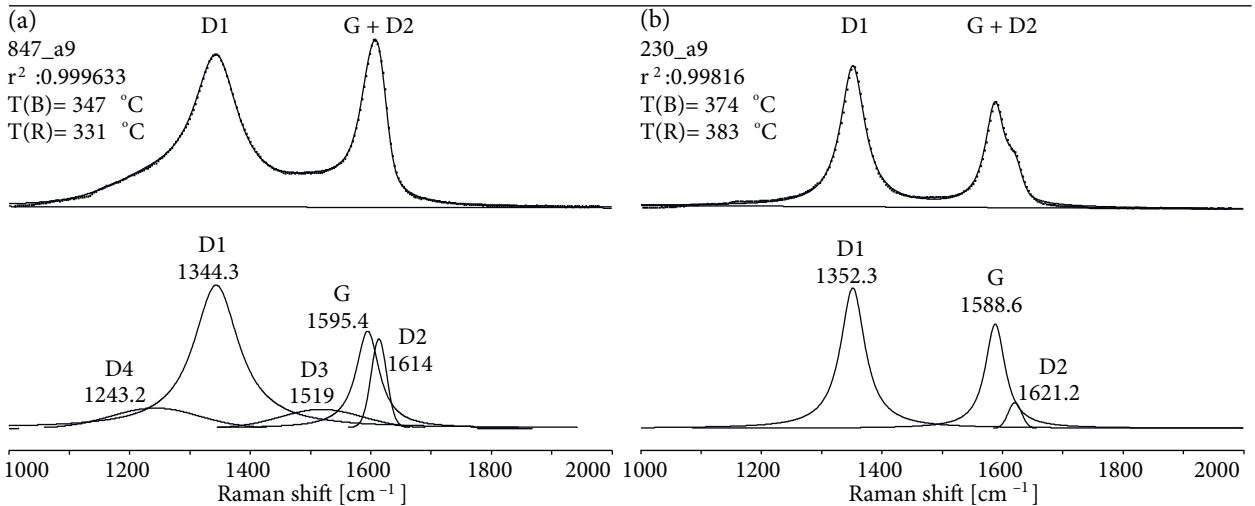
Figure 8. Representative examples of fitting of the measured Raman spectra. **a)** Low-temperature slates that are characterized by undifferentiating of graphite (G) and D2 defect bands and occurrence of large D3 and D4 defect bands (sample 847). **b)** Phyllite showing a slightly pronounced G band with D2 occurring on its shoulder (sample 230).

by subsequent or younger deformation events. RSCM of the metapelitic rocks provides temperature estimates that might be interpreted in terms of the structure of the Albian-Turonian accretionary wedge. Figure 10 shows the RSCM results contoured on the geological map of the studied area. The most striking aspect of the map is that the phyllites with higher metamorphic temperatures (370–385 °C) are exposed as a slice within the low-temperature slates (ca. 330 °C). The transition between phyllites and
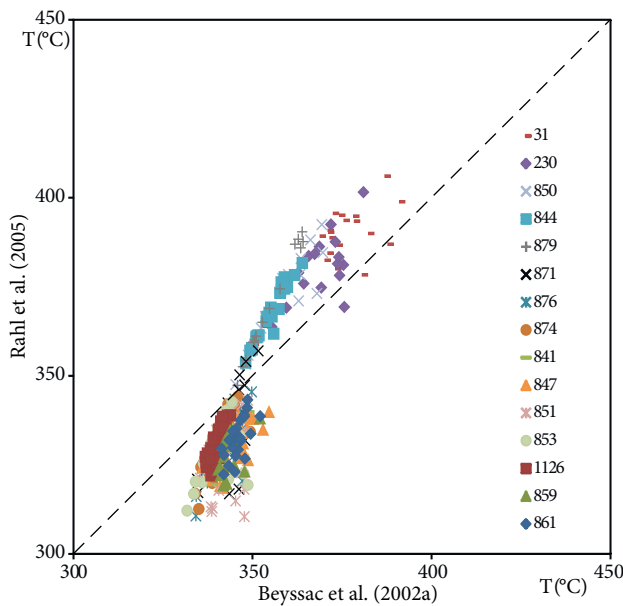
slate is nongradual, suggesting that they are juxtaposed tectonically. Na-amphibole bearing metabasites with similar foliation are exposed as a strip west of the phyllites. We infer that the phyllites are associated with these incipient blueschist facies metabasites. Sample 871 most probably represents a gradual increase in metamorphic temperature of the slates towards the contact with the Domuzdağ Complex. To the south of the studied area, however, the metaflysch sequence shows an inverted metamorphic grade, where phyllites structurally overlie the slates. This is related to postmetamorphic deformation along the Akçataş Fault causing underthrusting of the Esenler Unit beneath the Domuzdağ Complex.

A major portion of the wedge is formed by the low-temperature slates that possibly represent scraped off turbidites coming to the trench. The phyllites, however, most likely formed during shallow level underplating of continental detritus beneath the offscraped distal turbidites (Figure 11). The associated incipient blueschist facies metabasite strip was peeled off from the sinking oceanic crust and mixed tectonically with the phyllites during underplating along the basal décollement (Kimura and Ludden, 1995).

There are no kinematic data for the tectonic emplacement of the underplated phyllites into the offscraped turbidites. The youngest deformation in the studied area is represented by post-Eocene east-west striking oblique strike-slip faulting, which strongly modified the southern part of the area studied. The post-Eocene deformation is characterized by northward tilting and emplacement of the higher-grade Domuzdağ

Figure 9. Diagram showing RSCM temperatures obtained using calibrations of Beyssac et al. (2002a) and Rahl et al. (2005).

Table 2. The analytical data of the RSCM of the measured samples and the calculated mean temperature values.

Sample	#	G Position	1σ	G FWHM	1σ	D1 position	1σ	D1 FWHM	1σ	R1	1σ	R2	1σ	T^B (°C)	CI	1σ	T^R (°C)	CI	1σ
31	24	1587.46	0.63	35.88	1.72	1352.33	0.66	41.90	1.69	1.48	0.24	0.61	0.03	371	4	11	385	5	12
230	17	1588.08	1.13	37.57	1.77	1352.00	1.10	45.09	3.25	1.47	0.16	0.61	0.02	369	3	7	381	4	9
850	21	1588.82	0.78	44.04	0.99	1350.62	0.70	50.35	2.66	1.77	0.18	0.64	0.02	357	3	7	370	5	12
844	25	1587.98	1.00	41.24	1.29	1350.65	1.00	46.95	1.96	1.80	0.10	0.64	0.01	355	2	4	367	3	8
879	15	1590.24	0.93	43.30	2.19	1352.16	0.69	46.93	2.43	1.91	0.10	0.64	0.02	355	4	7	369	8	15
871	20	1590.15	1.88	47.73	2.38	1350.38	1.30	56.70	4.81	2.27	0.19	0.67	0.01	344	2	5	334	6	13
876	23	1594.27	2.35	46.48	5.55	1343.98	2.36	85.92	10.16	1.66	0.14	0.67	0.01	342	2	4	330	4	9
874	29	1596.56	0.97	44.73	1.91	1344.10	1.83	81.73	7.74	1.78	0.19	0.67	0.01	341	1	3	331	3	8
841	22	1595.57	1.10	42.98	1.91	1343.97	1.43	79.77	5.23	1.71	0.14	0.67	0.01	342	1	3	332	2	5
847	30	1595.31	1.11	46.30	3.41	1343.94	1.15	93.20	3.44	1.53	0.11	0.66	0.01	345	1	4	330	2	6
851	23	1595.04	1.13	45.84	4.07	1344.89	3.21	84.77	11.70	1.64	0.22	0.67	0.01	343	2	4	328	4	11
853	20	1596.01	1.35	45.36	2.64	1346.26	2.83	81.79	11.52	1.79	0.26	0.67	0.01	341	2	5	328	4	9
1126	26	1596.08	1.04	44.63	1.74	1346.44	0.80	77.49	3.90	1.83	0.15	0.68	0.01	340	1	2	331	2	5
859	19	1595.22	1.82	45.98	1.95	1346.80	1.48	82.82	5.59	1.55	0.08	0.67	0.01	344	1	3	328	3	6
861	23	1593.42	1.18	50.71	0.94	1345.82	0.66	94.46	2.30	1.54	0.07	0.66	0.01	346	1	3	332	2	6

is the amount of spectra used during temperature calculations; 1σ = standard deviation; CI = 95% confidence interval. Temperature values T^B based on calibrations of Beyssac et al. (2002a) and T^R on calibrations of Rahl et al. (2005).
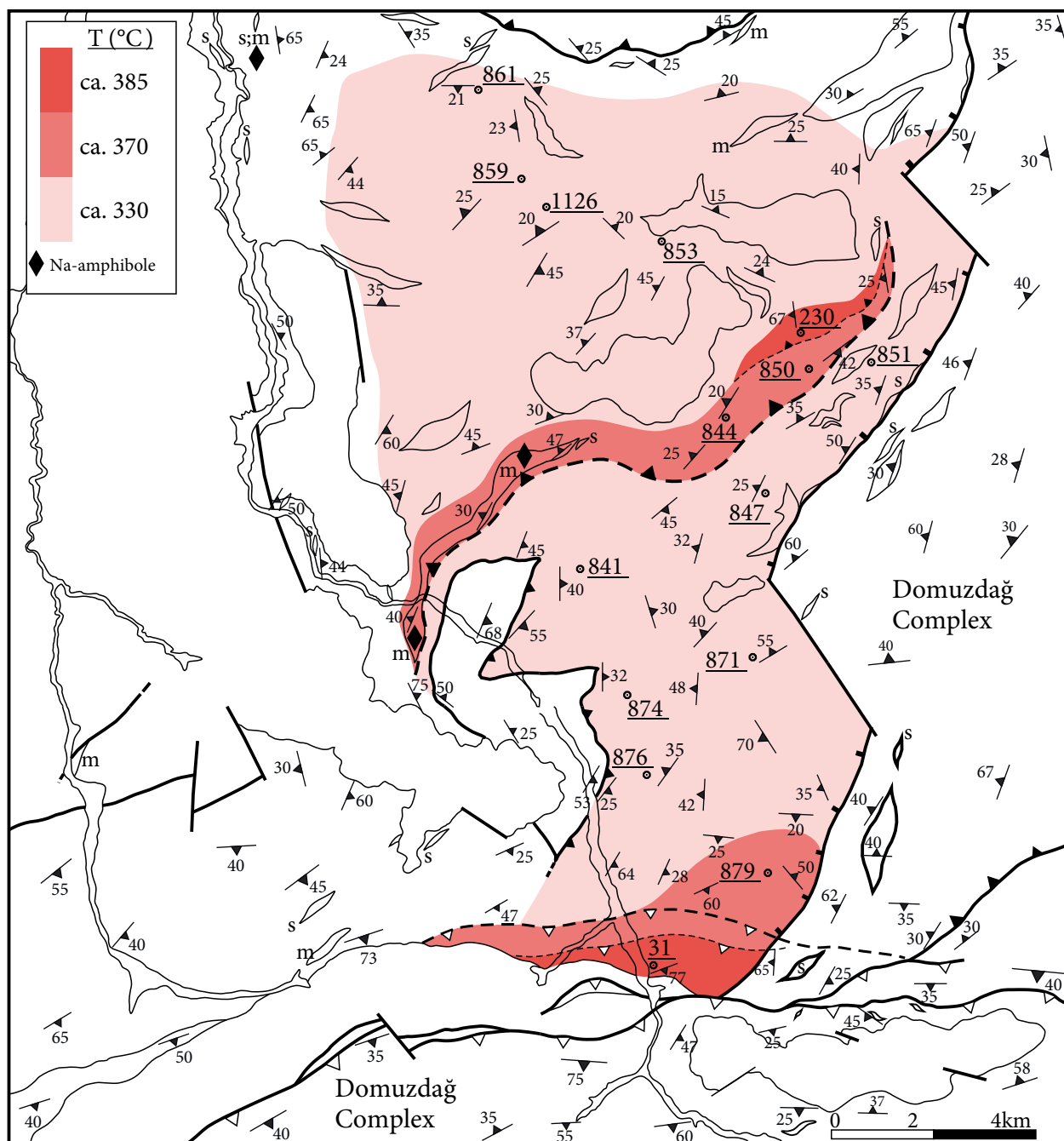
Figure 10. Thermal structure of the accreted distal turbidites produced by contouring the temperature values on the geological map of the area studied. The temperature values used are from the calibration of Rahl et al. (2005). Relatively high-temperature phyllites form a sliver within the low-temperature slates and are interpreted as a synconvergence out-of-sequence thrust.

Complex over the Esenler Unit. However, this northward tilting is absent in the phyllites that were exposed as a slice within the slates in the central part of the studied area. These phyllites and the associated metabasite strip show gently NW-dipping foliation planes similar to the general structural trend of the Albian-Turonian wedge. This

suggests that their tectonic emplacement occurred during synsubduction stacking.

In accretionary wedges, out-of-sequence thrusting is a common phenomenon in order to maintain the critical wedge taper during tectonic thickening of the wedge (Platt, 1986; Morley, 1988). It can juxtapose distinct
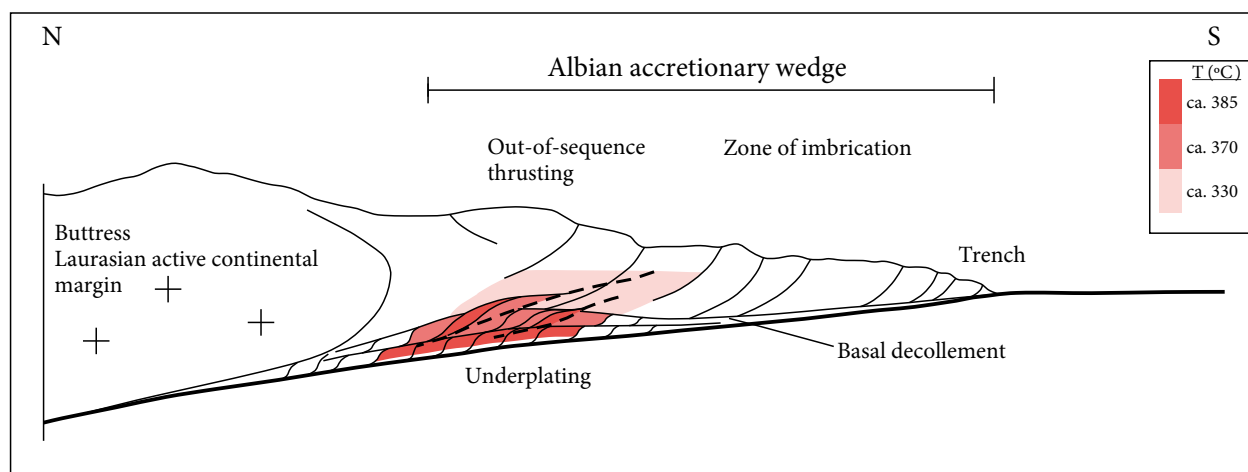
Figure 11. A model showing a possible initial situation of the phyllites and the slates within the Albian accretionary wedge. While the slates represent the offscraped distal turbidites, the phyllite possibly represents underplated metasediments of the turbidite fan. Out-of-sequence thrusting (dashed thick lines) is proposed for uplift and tectonic emplacement of the phyllites. The model is modified after Moore et al. (2001).

metamorphic piles during accretion within the wedge. Vitrinite reflectance studies revealed a sharp thermal discontinuity in the Cretaceous Shimanto accretionary complex, Japan, which is interpreted as an out-of-sequence thrust (Ohmori et al., 1997). Tectonic emplacement of the underplated phyllites and the Na-amphibole bearing metabasite strip within the lower-temperature offscraped slates is thus regarded as controlled by out-of-sequence thrusting causing tectonic thickening and uplift of the wedge (Figure 11).

6. Conclusions
Albian-Turonian subduction-accretionary complexes are exposed widely in the Central Pontides. To the north, the accretionary complexes are dominated by metaclastic rocks representing accreted distal parts of a large Lower Cretaceous submarine turbidite fan deposited on the Laurasian active continental margin. The metaclastic sequence is a low-grade HP metaflysch consisting of slate/phyllite and metasandstone intercalation with extensive blocks of marble, Na-amphibole bearing metabasite, and serpentinite. The metamorphic temperatures in the metapelitic rocks were investigated using Raman spectroscopy of carbonaceous material. The majority of the metapelites are low-temperature slates with peak metamorphic temperature of ca. 330 °C. The rocks

possibly represent offscraped distal turbidites along the toe of the Albian-Turonian accretionary wedge. The rest are phyllites and their peak metamorphic temperatures are constrained to 370–385 °C. The phyllites occur as a sliver within the low-temperature offscraped turbidites together with a strip of Na-amphibole-bearing metabasite. We interpret the phyllites as underplated continental detritus along the basal décollement together with the metabasite strip, which was peeled off from the sinking oceanic crust. Hence, the Albian-Turonian accretionary wedge comprises both offscraped and shallow level underplated distal turbidites with distinct peak metamorphic temperatures that caused frontal accretionary growth of the Laurasian active margin. Juxtapositioning of the offscraped and underplated parts of the wedge was possibly controlled by out-of-sequence thrusting, causing tectonic thickening and uplift of the wedge.

References

Altherr R, Topuz G, Marschall H, Zack T, Ludwig T (2004). Evolution of a tourmaline-bearing lawsonite eclogite from the Elekdag area (Central Pontides, N Turkey): evidence for infiltration of slab-derived B-rich fluids during exhumation. Contrib Mineral Petr 148: 409–425.

Aoya M, Kouketsu Y, Endo S, Shimizu H, Mizukami T, Nakamura D, Wallis S (2010). Extending the applicability of the Raman carbonaceous-material geothermometer using data from contact metamorphic rocks. J Metamorph Geol 28: 895–914.

Aygül M, Okay AI, Oberhänsli R, Sudo M (2015a). Pre-collisional accretionary growth of the southern Laurasian margin, Central Pontides, Turkey. Tectonophysics (submitted).

Aygül M, Okay AI, Oberhänsli R, Schmidt A, Sudo M (2015b). Late Cretaceous infant intra-oceanic arc volcanism, the Central Pontides, Turkey: petrogenetic and tectonic implications. J Asian Earth Sci (in press).

Barkurt MY, Bilginer E, Pehlivan Ş, Örçen S (1990). Geology of the Kastamonu-Ovacık Region. Ankara, Turkey: MTA Report No. 9079 (in Turkish).

Beyssac O, Bollinger L, Avouac JP, Goffe B (2004). Thermal metamorphism in the Lesser Himalaya of Nepal determined from Raman spectroscopy of carbonaceous material. Earth Planet Sci Lett 225: 233–241.

Beyssac O, Goffé B, Chopin C, Rouzaud JN (2002a). Raman spectra of carbonaceous material in metasediments: a new geothermometer. J Metamorph Geol 20: 859–871.

Beyssac O, Rouzaud JN, Goffé B, Brunet F, Chopin C (2002b). Characterization of high-pressure, low-temperature graphitization: a Raman microspectroscopy and HRTEM study. Contrib Mineral Petr 143: 19–31.

Beyssac O, Simoes M, Avouac JP, Farley KA, Chen YG, Chan YC, Goffe B (2007). Late Cenozoic metamorphic evolution and exhumation of Taiwan. Tectonics 26: TC6001.

Boztuğ D (1992). Daday-Devrekani Masifi güney kesiminin litostratigrafi birimleri ve tektoniği. MTA Dergisi 114: 1–20 (in Turkish).

Chen F, Siebel W, Satır M, Terzioğlu N, Saka K (2002). Geochronology of the Karadere basement (NW Turkey) and implications for the geological evolution of the İstanbul Zone. Int J Earth Sci 91: 469–481.

Dean WT, Monod O, Rickards RB, Demir O, Bultynck P (2000). Lower Palaeozoic stratigraphy and palaeontology, Karadere-Zirze area, Pontus Mountains, northern Turkey. Geol Mag 137: 555–582.

Diessel CFK, Brothers NR, Black PM (1978). Coalification and graphitization in high-pressure schists in New Caledonia. Contrib Mineral Petr 68: 63–78.

Görür N (1988). Timing of opening of the Black Sea basin. Tectonophysics 147: 247–262.

Hippolyte JC, Müller C, Kaymakçı N, Sangu E (2010). Dating of the Black Sea Basin: new nannoplankton ages from its inverted margin in the Central Pontides (Turkey). In: Sosson M, Kaymakci N, Stephenson RA, Bergerat F, Starostenko V, editors. Sedimentary Basin Tectonics from the Black Sea and Caucasus to the Arabian Platform. London, UK: Geological Society of London Special Publications, pp. 113–136.

Itaya T (1981). Carbonaceous material in pelitic schists of the Sanbagawa metamorphic belt in central Shikoku, Japan. Lithos 14: 215–224.

Karig DE, Sharman GF (1975). Subduction and accretion in trenches. Geol Soc Am Bull 86: 377–389.

Kimura G, Ludden J (1995). Peeling oceanic crust in subduction zones. Geology 23: 217–220.

Lahfid A, Beyssac O, Deville E, Negro F, Chopin C, Goffé B (2010). Evolution of the Raman spectrum of carbonaceous material in low-grade metasediments of the Glarus Alps (Switzerland). Terra Nova 22: 354–360.

Landis CA (1971). Graphitization of dispersed carbonaceous materials in metamorphic rocks. Contrib Mineral Petr 30: 34–45.

Marroni M, Frassi C, Göncüoglu MC, Di Vincenzo G, Pandolfi L, Rebay G, Ellero A, Ottria G (2014). Late Jurassic amphibolite-facies metamorphism in the Intra-Pontide Suture Zone (Turkey): an eastward extension of the Vardar Ocean from the Balkans into Anatolia? J Geol Soc London 171: 605–608.

McCall GJH (2002). A summary of the geology of the Iranian Makran. In: Clift PD, Kroon D, Gaedicke C, Craig J, editors. The Tectonic and Climatic Evolution of the Arabian Sea Region. London, UK: Geological Society of London Special Publications, pp. 147–204.

Meijers MJM, Vrouwe B, van Hinsbergen DJJ, Kuiper KF, Wijbrans J, Davies GR, Stephenson RA, Kaymakcı N, Matenco L, Saintot A (2010). Jurassic arc volcanism on Crimea (Ukraine): implications for the paleo-subduction zone configuration of the Black Sea region. Lithos 119: 412–426.

Moore GF, Taira A, Klaus A, Becker L, Boeckel B, Cragg BA, Dean A, Fergusson CL, Henry P, Hirano S et al. (2001). New insights into deformation and fluid flow processes in the Nankai Trough accretionary prism: results of Ocean Drilling Program Leg 190. Geochem Geophy Geosy 2: 1058.

Morley CK (1988). Out-of-sequence thrusts. Tectonics 7: 539–561.

Nemanich RJ, Solin SA (1979). First- and second-order Raman scattering from finite-size crystals of graphite. Phys Rev B 20: 392–401.

Nikishin AM, Okay AI, Tüysüz O, Demirer A, Wannier M, Amelin N, Petrov E (2015). The Black Sea basins structure and history: new model based on new deep penetration regional seismic data. Part 2: tectonic history and paleogeography. Mar Petrol Geol 59: 656–670.

Nzegge OM, Satır M, Siebel W, Taubald H (2006). Geochemical and isotopic constraints on the genesis of the Late Palaeozoic Deliktas̨ and Sivrikaya granites from the Kastamonu granitoid belt (Central Pontides, Turkey). Neues Jb Miner Abh 183: 27–40.

Ohmori K, Taira A, Tokuyama H, Sakaguchi A, Okamura M, Aihara A (1997). Paleothermal structure of the Shimanto accretionary prism, Shikoku, Japan: role of an out-of-sequence thrust. Geology 25: 327–330.

Okay AI, Altıner D, Kılıç AM (2015). Triassic limestone, turbidites and serpentinite–the Cimmeride orogeny in the Central Pontides. Geol Mag 152: 460–479.

Okay AI, Nikishin AM (2015). Tectonic evolution of the southern margin of Laurasia in the Black Sea region. Int Geol Rev 57: 1051–1076.

Okay AI, Şengör AMC, Görür N (1994). Kinematic history of the opening of the Black Sea and its effect on the surrounding regions. Geology 22: 267–270.

Okay AI, Sunal G, Sherlock S, Altıner D, Tüysüz O, Kylander-Clark ARC, Aygül M (2013). Early Cretaceous sedimentation and orogeny on the active margin of Eurasia: Southern Central Pontides, Turkey. Tectonics 32: 1247–1271.

Okay AI, Sunal G, Tüysüz O, Sherlock S, Keskin M, Kylander-Clark ARC (2014). Low-pressure–high-temperature metamorphism during extension in a Jurassic magmatic arc, Central Pontides, Turkey. J Metamorph Geol 32: 49–69.

Okay AI, Tüysüz O (1999). Tethyan sutures of northern Turkey. In: Durand B, Jolivet L, Horvath F, Seranne M, editors. The Mediterranean Basins: Tertiary Extension within the Alpine Orogen. London, UK: Geological Society of London Special Publications, pp. 475–515.

Okay AI, Tüysüz O, Satır M, Özkan-Altıner S, Altıner D, Sherlock S, Eren RH (2006). Cretaceous and Triassic subduction-accretion, HP/LT metamorphism and continental growth in the Central Pontides, Turkey. Geol Soc Am Bull 118: 1247–1269.

Pasteris JD (1989). In situ analysis in geological thin-sections by Laser Raman microprobe microspectroscopy: a cautionary note. Appl Spectrosc 43: 567–570.

Pasteris JD, Wopenka B (1991). Raman spectra of graphite as indicators of degree of metamorphism. Can Mineral 29: 1–9.

Platt JP (1986). Dynamics of orogenic wedges and the uplift of high-pressure metamorphic rocks. Geol Soc Am Bull 97: 1037–1053.

Platt JP, Leggett JK, Young J, Raza H, Alam S (1985). Large scale sediment underplating in the Makran accretionary prism, southwest Pakistan. Geology 13: 507–511.

Rahl JM, Anderson KM, Brandon MT, Fassoulas C (2005). Raman spectroscopic carbonaceous material thermometry of low-grade metamorphic rocks: calibration and application to tectonic exhumation in Crete, Greece. Earth Planet Sci Lett 240: 339–354.

Sadezky A, Muckenhuber H, Grothe H, Niessner R, Pöschl U (2005). Raman microspectroscopy of soot and related carbonaceous materials: spectral analysis and structural information. Carbon 43: 1731–1742.

Sample JC, Fisher DM (1986). Duplex accretion and underplating in an ancient accretionary complex, Kodiak Islands, Alaska. Geology 14: 160–163.

Scharf A, Handy MR, Ziemann MA, Schmid SM (2013). Peak-temperature patterns of polyphase metamorphism resulting from accretion, subduction and collision (eastern Tauern Window, European Alps) – a study with Raman microspectroscopy on carbonaceous material (RSCM). J Metamorph Geol 31: 863–880.

Tissot BP, Welte DH (1978). Petroleum Formation and Occurrence. A New Approach to Oil and Gas Exploration. 1st ed. Heidelberg, Germany: Springer-Verlag.

Topuz G, Göçmengil G, Rolland Y, Çelik ÖF, Zack T, Schmitt AK (2013). Jurassic accretionary complex and ophiolite from northeast Turkey: no evidence for the Cimmerian continental ribbon. Geology 41: 255–258.

Tuinstra F, Koenig JL (1970). Raman spectrum of graphite. J Chem Phys 53: 1126–1130.

Tüysüz O (1990). Tectonic evolution of a part of the Tethyside orogenic collage: the Kargı Massif, northern Turkey. Tectonics 9: 141–160.

Tüysüz O (1999). Geology of the Cretaceous sedimentary basins of the Western Pontides. Geol J 34: 75–93.

Tüysüz O, Tekin UK (2007). Timing of imbrication of an active continental margin facing the northern branch of Neotethys, Kargı Massif, northern Turkey. Cretaceous Res 28: 754–764.

Uğuz MF, Sevin M, Duru M (2002). Geological Map of Turkey. 1: 500.000 Scaled Sinop Sheet. Ankara, Turkey: MTA.

Ustaömer T, Robertson AHF (1993). A Late Paleozoic-Early Mesozoic marginal basin along the active southern continental margin of Eurasia: evidence from the Central Pontides (Turkey) and adjacent regions. Geol J 28: 219–238.

Ustaömer T, Robertson AHF (1994). Late Paleozoic marginal basin and subduction-accretion: the Paleotethyan Küre Complex, Central Pontides, northern Turkey. J Geol Soc London 151: 291–305.

Ustaömer T, Robertson AHF (1997). Tectonic-sedimentary evolution of the North-Tethyan margin in the Central Pontides of northern Turkey. In: Robinson, AG, editor. Regional and Petroleum Geology of the Black Sea and Surrounding Region. Tulsa, OK, USA: AAPG, pp. 255–290.

Ustaömer T, Robertson AHF (1999). Geochemical evidence used to test alternative plate tectonic models for pre-Upper Jurassic (Palaeotethyan) units in the Central Pontides, N Turkey. Geol J 34: 25–53.

von Huene R, Scholl DW (1991). Observations at convergent margins concerning sediment subduction, subduction erosion, and the growth of continental crust. Rev Geophys 3: 279–316.

Yılmaz O, Boztuğ D (1986). Kastamonu granitoid belt of northern Turkey: first arc plutonism product related to the subduction of the Paleo-Tethys. Geology 14: 179–183.

Yui TF, Huang E, Xu J (1996). Raman spectrum of carbonaceous material: a possible metamorphic grade indicator for low-grade metamorphic rocks. J Metamorph Geol 14: 115–124.

Wopenka B, Pasteris JD (1993). Structural characterization of kerogens to granulite-facies graphite: applicability of Raman microprobe spectroscopy. Am Mineral 78: 533–557.